**Contents**

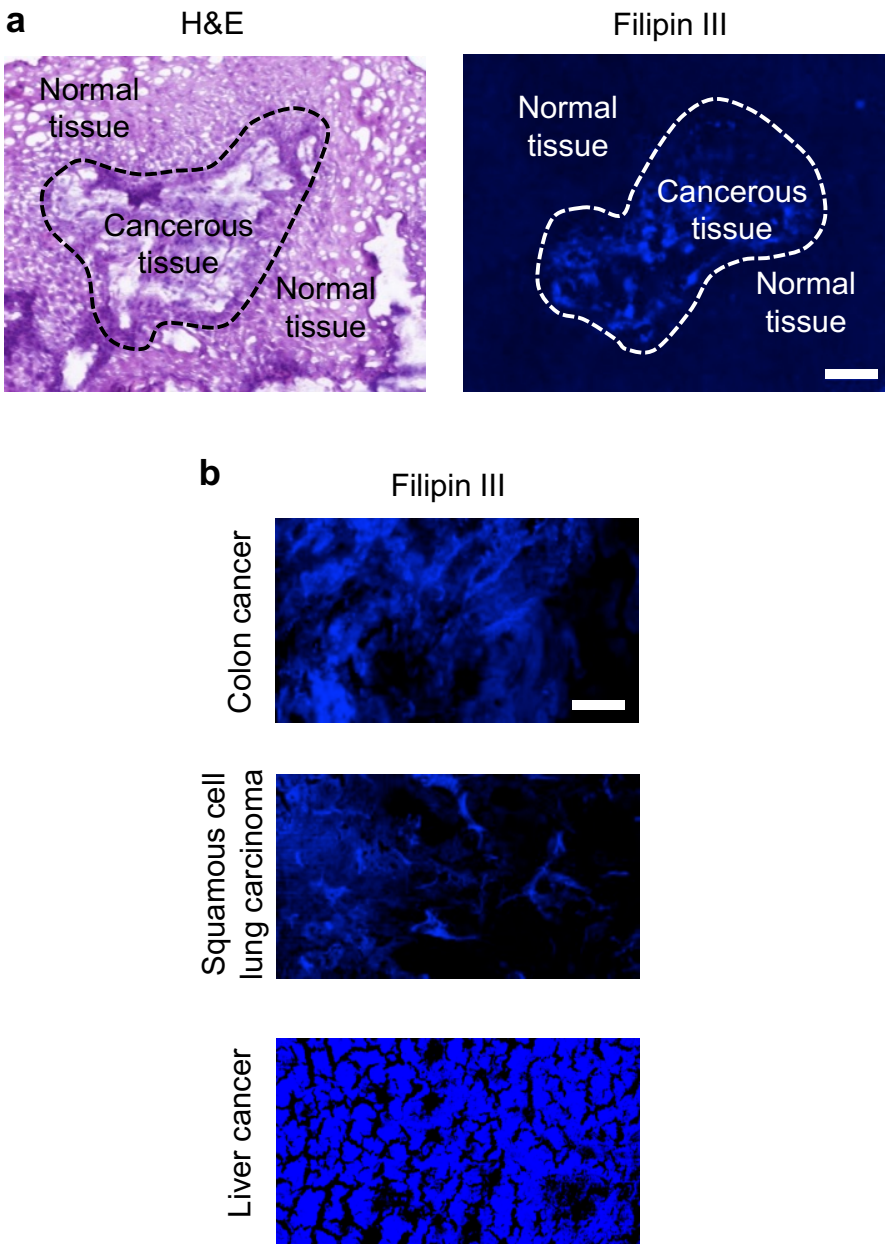


**Supplementary Figure 1**

**Cholesterol level is upregulated in various human cancer tissues.**

**a**, Human small cell lung cancer tissue (indicated within the dash line) and its adjacent normal tissue from a patient were stained with hematoxylin and eosin (H&E) and Filipin III (shown in blue colour). Scale bar, 100 μm. **b**, Filipin III staining (shown in blue colour) of human colon cancer, squamous cell lung carcinoma, and liver cancer biopsies from patients. Scale bar, 100 μm.

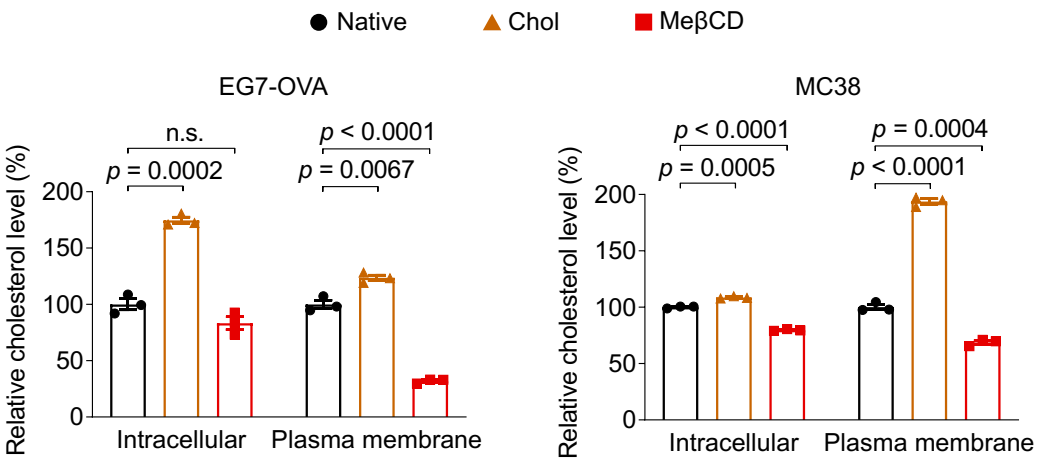


**Supplementary Figure 2**

**Treatment of water-soluble cholesterol/methyl-β-cyclodextrin complex (Chol) or methyl-β-cyclodextrin (MeβCD) significantly increases or decreases cholesterol levels in plasma membrane of various cancer cells, respectively.**

Relative intracellular and plasma membrane cholesterol levels of native, Chol (5 mM), and MeβCD (5 mM)-treated cancer cells at 37 °C for 30 min (n = 3). Native cancer cells serve as a standard (100%). Data are one representative of two independent experiments with biological replicates. *P* values were determined by unpaired Student's *t* test. Error bars represent standard error of the mean (SEM). n.s., not significant.

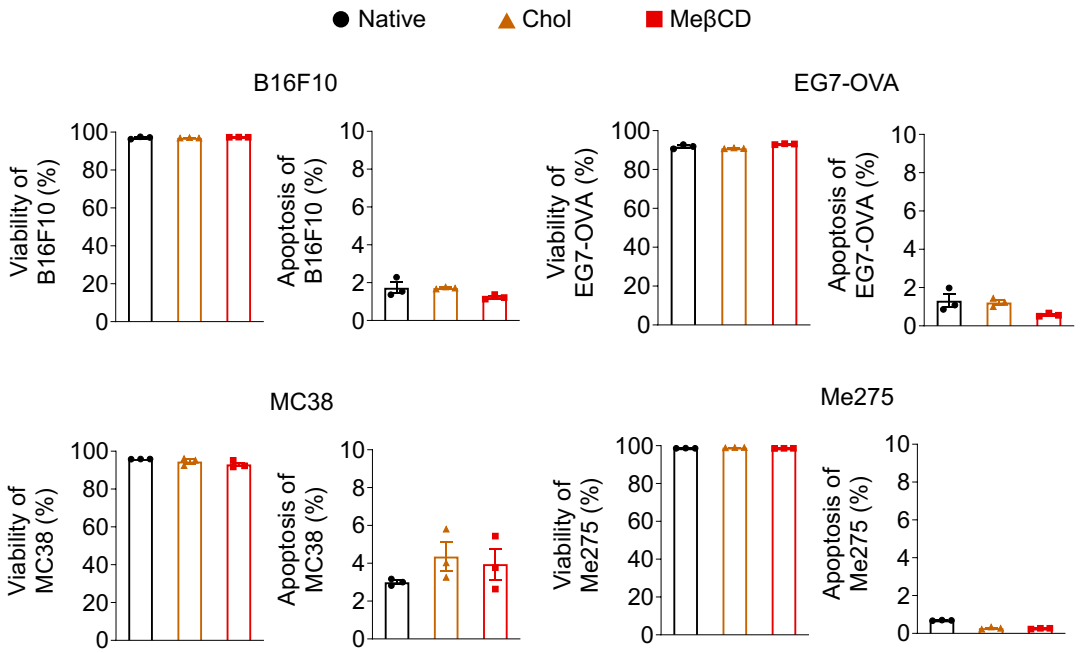


**Supplementary Figure 3**

**Treatment of Chol or MeβCD shows negligible impacts on the viability or apoptosis of various cancer cell lines.**

Viability and apoptosis percentage of indicated cancer cell lines after treatment with Chol (5 mM) or MeβCD (5 mM) at 37 °C for 30 min (n = 3). Data are one representative of at least two independent experiments with biological replicates. Error bars represent SEM.

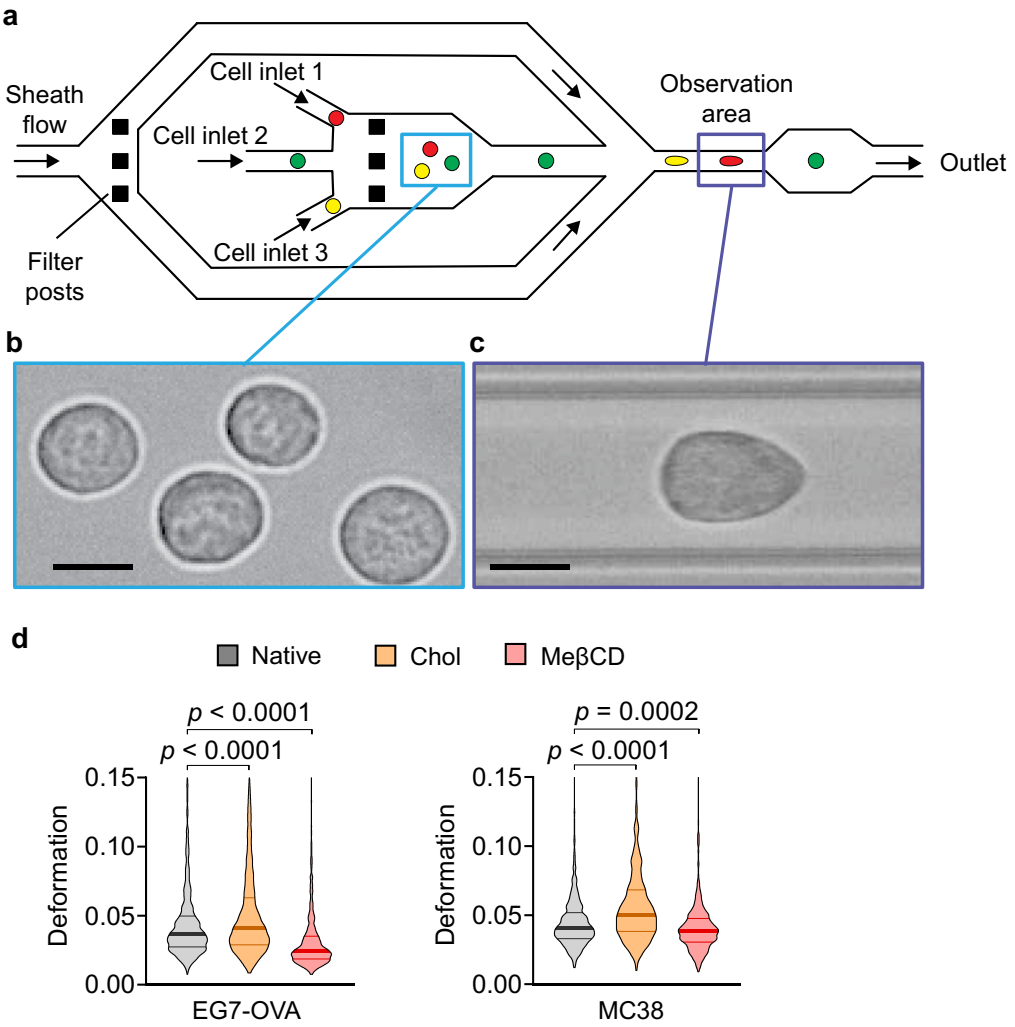


**Supplementary Figure 4**

**Treatment of Chol or MeβCD softens or stiffens various cancer cells, respectively, measured by deformability cytometry (DC).**

**a**, Schematic illustration of the microfluidic device for DC. The deformation of native, Chol-, and MeβCD-treated cancer cells were measured using the same microfluidic device that has three inlets dedicated for different groups. Cells from different groups were introduced through the designated inlets in sequence and the cell deformation generated by the sheath flow was recorded in the observation area. Microfabricated posts serve as size-selective filters to remove cell aggregates. **b**, A representative image of the cells before they were introduced to the constriction showing that the majority of cells had round shapes. Scale bars, 15 μm. **c**, A representative image of a deformed cell that is passing through the observation area. The cells display a characteristic bullet shape because they were deformed by shear stresses and pressure gradients. Scale bars, 15 μm. **d**, Quantitative cell deformation of native, Chol-, and MeβCD-treated EG7-OVA (n = 2026, 1947, and 1947, respectively) or MC38 (n = 999 for each group) cancer cells (outliers not shown). In the violin plots, the middle solid line shows median, and lower and upper dash lines show 25$^{th}$ and 75$^{th}$ percentiles, respectively. *P* values were determined by unpaired Student's *t* test.

**a**

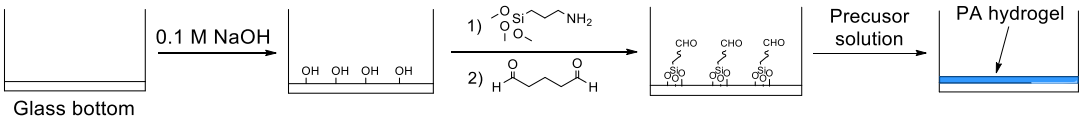


**b**

| Sample | Acrylamide (w/v %) | Bis-acrylamide (w/v %) | Young's Modulus (kPa) |
|---|---|---|---|
| PA-1 | 10 | 0.35 | 55 ± 3 |
| PA-2 | 18 | 0.38 | 143 ± 5 |
| PA-3 | 4 | 0.10 | 0.26 ± 0.01 |
| PA-4 | 4 | 0.11 | 0.51 ± 0.07 |
| PA-5 | 4 | 0.13 | 0.89 ± 0.02 |

**Supplementary Figure 5**

**Syntheses and characterizations of polyacrylamide (PA) hydrogels.**

**a**, Schematic illustration of the fabrication process of PA hydrogels on a glass-bottom well plate. **b**, Summary of the compositions and Young's modulus of PA hydrogel substrates (n = 3 independent samples).

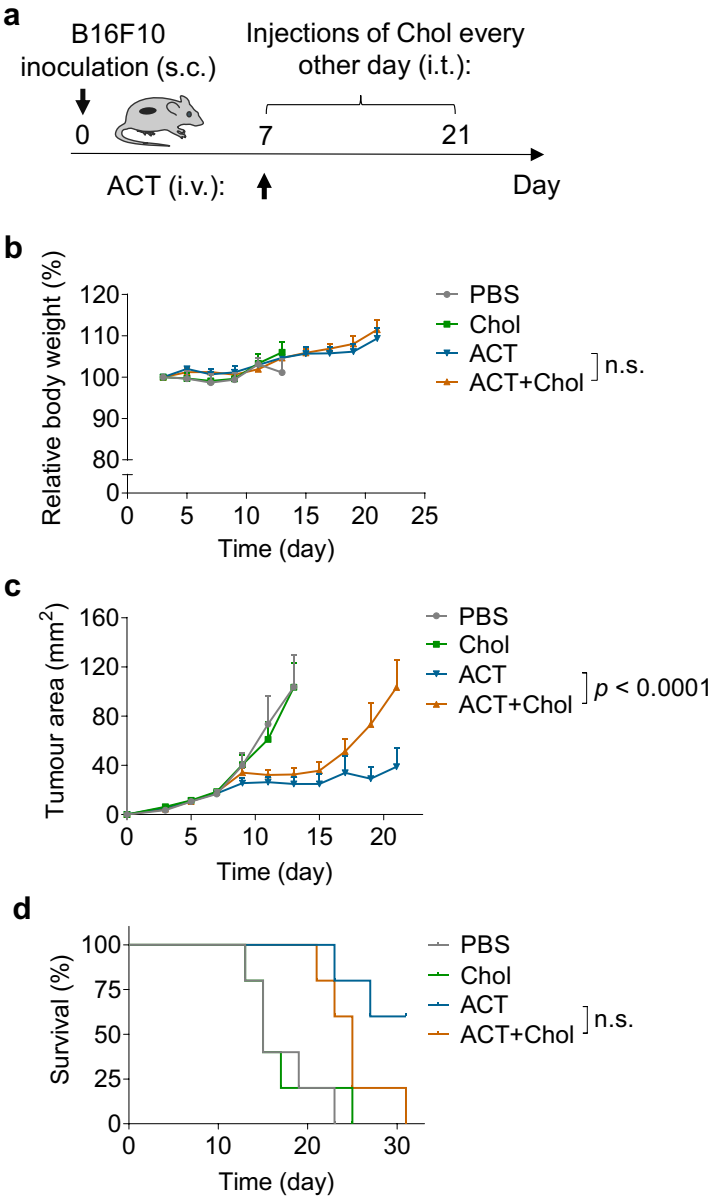


**Supplementary Figure 6**

**Cancer-cell softening by supplementing cholesterol impairs the anti-tumour efficacy of adoptive T-cell transfer (ACT) therapy in vivo.**

**a-d**, C57BL/6 mice were inoculated subcutaneously (s.c.) with B16F10 cancer cells ($0.5 \times 10^6$ per mouse) at day 0, and received intravenous (i.v.) adoptive transfer of activated Pmel $CD8^+$ T-cells ($5 \times 10^6$ per mouse) at day 7 followed by intratumoural (i.t.) administration of Chol (2 mg per injection) or PBS every other day from day 7 to 21. B16F10 tumour-bearing mice receiving i.t. administration of PBS or Chol only (2 mg per injection) every other day from day 7 to 21 serve as controls. Experimental scheme (**a**). Shown are relative body weights (**b**), tumour growth curves (**c**), and survival curves (**d**) (n = 5 animals per group). Data are one representative of two independent experiments. *P* values were determined by two-way ANOVA in (**b**, **c**), or log-rank test in (**d**). Error bars represent SEM. PBS, phosphate-buffered saline; n.s., not significant.

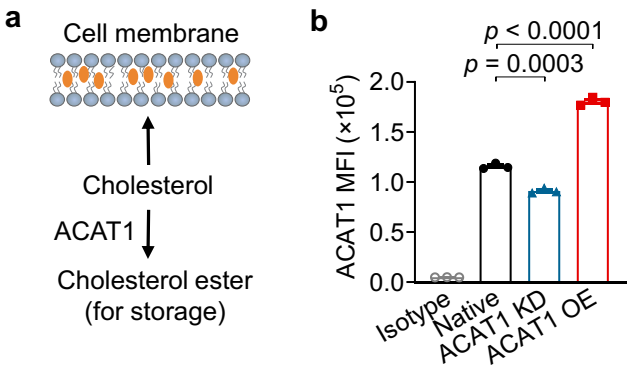


**Supplementary Figure 7**

**Regulation of acyl-CoA:cholesterol acyltransferase 1 (ACAT1) level through genetic modification in cancer cells.**

**a**, Schematic illustration of regulating membrane cholesterol levels through ACAT1. **b**, ACAT1 expression levels in native, ACAT1 knock-down (ACAT1 KD), and ACAT1 overexpressing (ACAT1 OE) B16F10 cancer cells detected by antibody staining and flow cytometry analysis (n = 3). Data are one representative of two independent experiments with biological replicates. *P* values were determined by unpaired Student's *t* test in (**b**). Error bars represent SEM. MFI, mean fluorescence intensity.

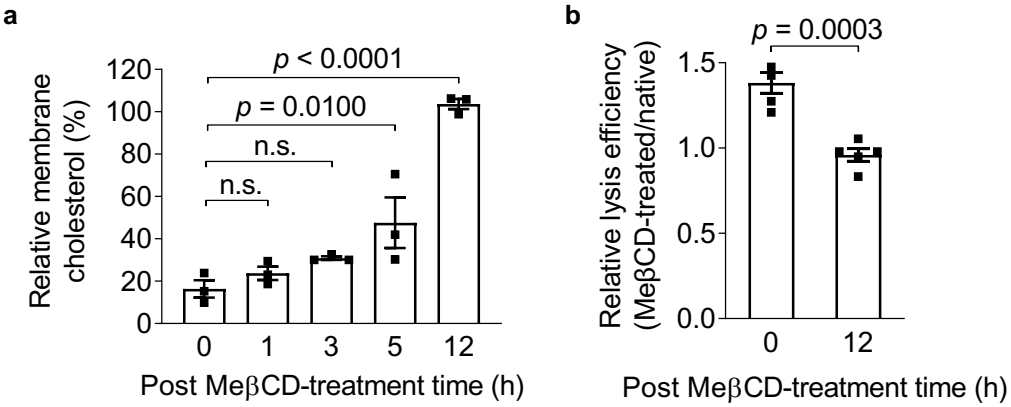


**Supplementary Figure 8**

**Kinetics of cholesterol levels in plasma membrane of B16F10 cancer cells post the treatment of MeβCD and its impact on T-cell mediated cytotoxicity.**

**a**, Relative membrane cholesterol levels of MeβCD-treated B16F10 cancer cells at indicated time points post treatment (n = 3). Membrane cholesterol level of native B16F10 serves as a standard (100%). **b**, Relative lysis efficiency of MeβCD-treated B16F10 cancer cells (0 or 12 h post treatment) co-cultured with activated Pmel $CD8^+$ T-cells at an effector:target ratio of 10:1 for 5 h (n = 5). Relative lysis efficiency was calculated by normalizing the lysis percentages by the mean value of native B16F10 cancer cells. Data are one representative of two independent experiments with biological replicates. *P* values were determined by unpaired Student's *t* test. Error bars represent SEM. n.s., not significant.

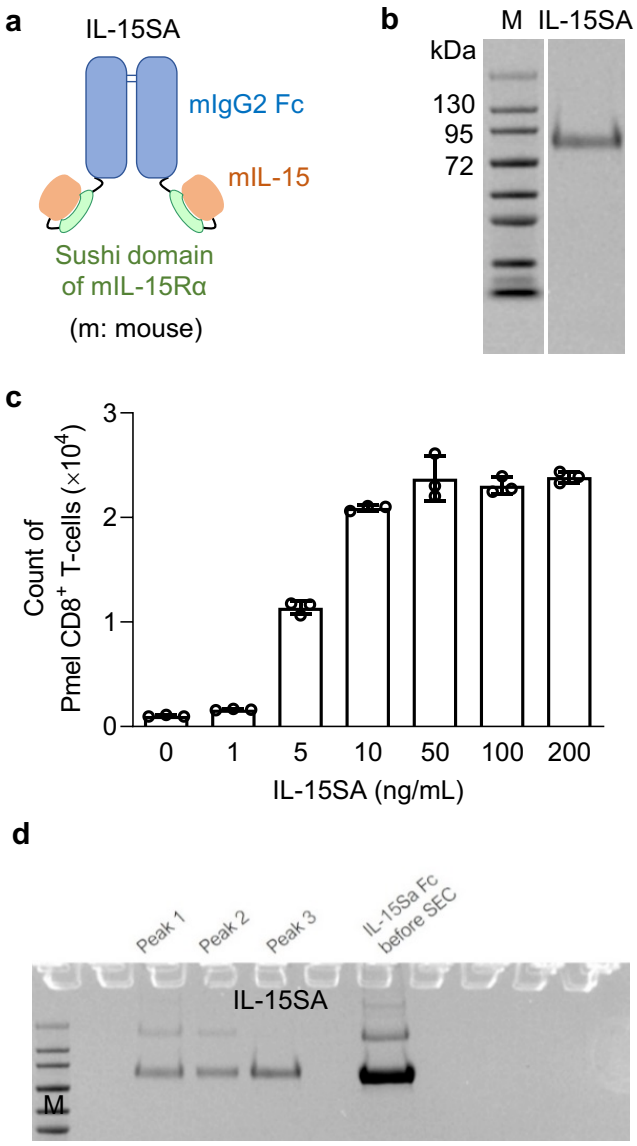


**Supplementary Figure 9**

**Production and characterizations of mouse interleukin-15 super-agonist (IL-15SA).**

**a**, Schematic diagram of the protein structure of IL-15SA. **b**, Representative sodium dodecyl sulfate-polyacrylamide gel electrophoresis (SDS-PAGE) analysis of the purified IL-15SA. **c**, Activated Pmel CD8+ T-cells ($5 \times 10^3$) were cultured in complete RPMI 1640 medium supplemented with IL-15SA at the indicated concentrations for 2 days (n = 3). Counts of T-cells were determined with flow cytometry. Data are one representative of two independent experiments with biological replicates. Error bars represent SEM. **d**, Unprocessed SDS-PAGE gel image for (**b**). M, prestained protein marker; kDa, kilodalton.

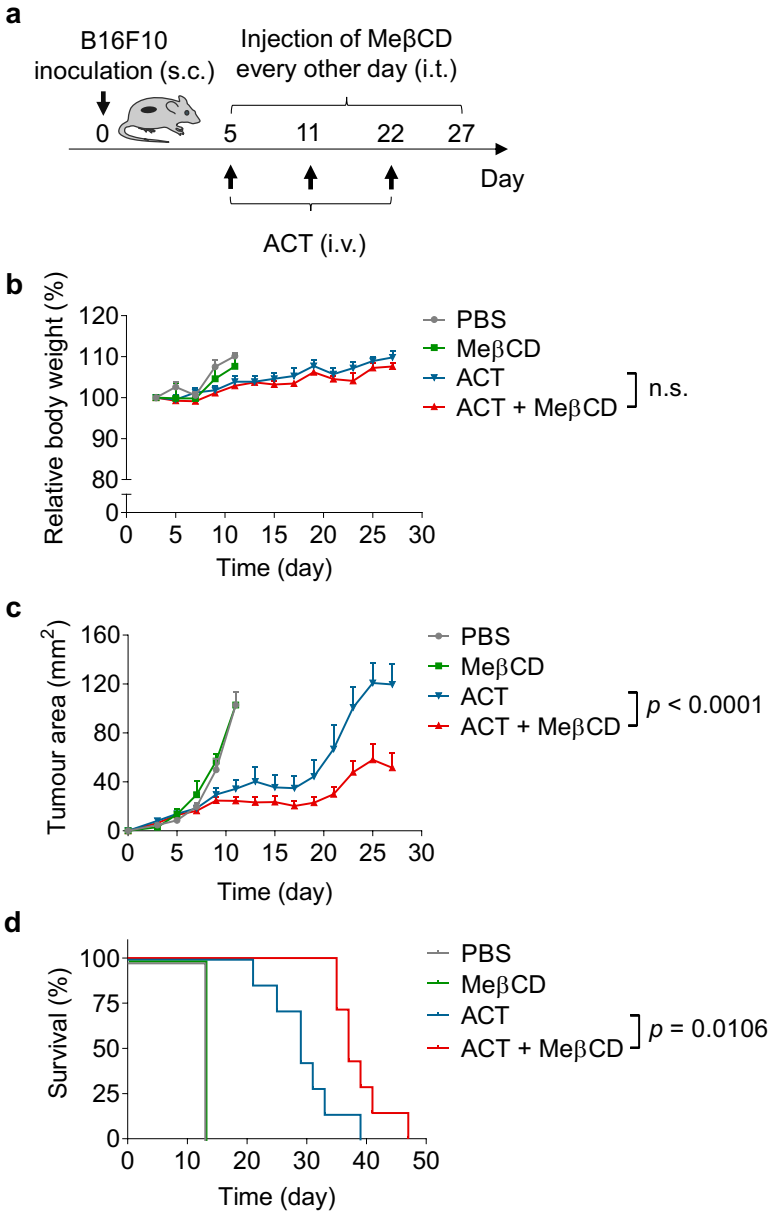


**Supplementary Figure 10**

**Cancer-cell stiffening using MeβCD enhances the anti-tumour efficacy of ACT therapy in mice bearing B16F10 tumours.**

**a-d**, C57BL/6 mice were inoculated subcutaneously (s.c.) with B16F10 tumour cells ($0.5 \times 10^6$ per mouse) at day 0, and received intravenous (i.v.) adoptive transfer of activated Pmel $CD8^+$ T-cells ($5 \times 10^6$ per injection) at day 5, 11, and 22, followed by intratumoural (i.t.) administration of MeβCD (2 mg per injection) or PBS every other day from day 5 to 27. B16F10 tumour-bearing mice receiving i.t. administration of PBS or MeβCD only (2 mg per injection) every other day from day 5 to 27 serve as controls. Experimental scheme (**a**). Shown are relative body weights (**b**), tumour growths (**c**), and survival curves (**d**) (n = 3 mice for PBS and MeβCD groups, and 7 mice for ACT and ACT + MeβCD groups). Data are one representative of two independent experiments with biological replicates. *P* values were determined by two-way ANOVA in (**b**, **c**), or log-rank test in (**d**). Error bars represent SEM. PBS, phosphate-buffered saline; n.s., not significant.

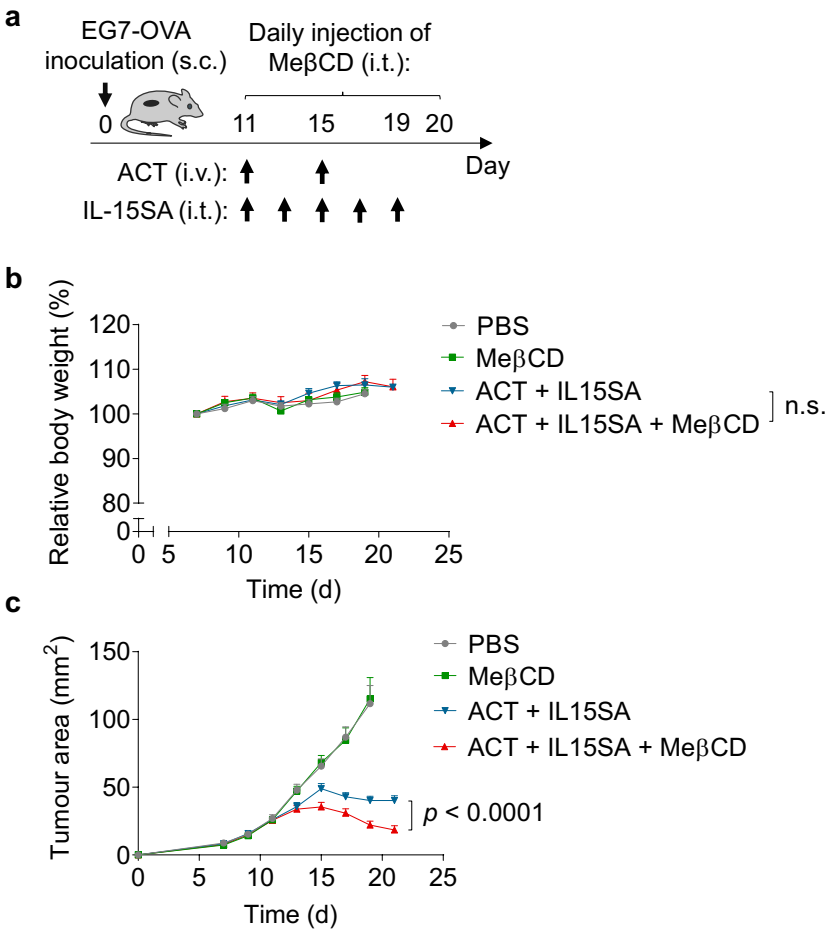


**Supplementary Figure 11**

**Cancer-cell stiffening using MeβCD enhances the anti-tumour efficacy of ACT therapy in mice bearing EG7-OVA tumours.**

**a-c**, C57BL/6 mice were inoculated subcutaneously (s.c.) with EG7-OVA tumour cells ($0.5 \times 10^6$ per mouse) at day 0, and received intravenous (i.v.) adoptive transfer of activated OT-I $CD8^+$ T-cells ($5 \times 10^6$ per injection) at day 11 and 15, followed by intratumoural (i.t.) administration of IL-15SA (5 µg per injection) every other day from day 11 to 19, and daily i.t. administration of MeβCD (1 mg per injection) or PBS from day 11 to 20. EG7-OVA tumour-bearing mice receiving daily i.t. administration of PBS or MeβCD (1 mg per injection) only from day 11 to 20 serve as controls. Experimental scheme (**a**). Shown are relative body weights (**b**) and tumour growths (**c**) (n = 10 animals per group). Shown are pooled data of two independent experiments with biological replicates. *P* values were determined by two-way ANOVA. Error bars represent SEM. PBS, phosphate-buffered saline; n.s., not significant.

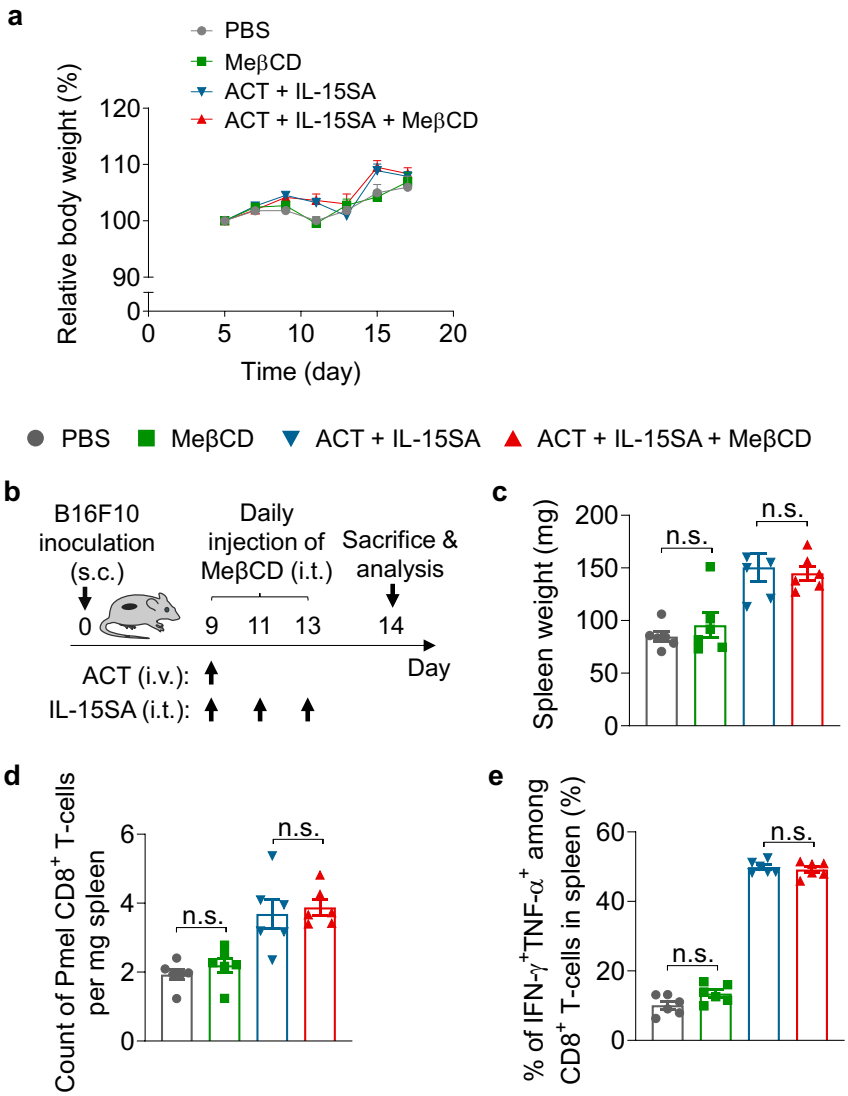


**Supplementary Figure 12**

**Treatment of MeβCD shows no overt systemic toxicity in mice.**

**a**, B16F10 tumour-bearing mice received the same treatment as shown in Figure 4c. Shown is relative body weights (n = 12 animals per group). Shown are pooled data of two independent experiments. **b**-**e**, C57BL/6 mice were inoculated subcutaneously (s.c.) with B16F10 tumour cells ($0.5 \times 10^6$ per mouse) at day 0, and received intravenous (i.v.) adoptive transfer of activated Pmel $CD8^+$ T-cells ($5 \times 10^6$ per mouse) at day 9, followed by intratumoural (i.t.) administration of IL-15SA (5 µg per injection) at day 9, 11, and 13, and daily i.t. administration of MeβCD (1 mg per injection) or PBS from day 9 to 13. B16F10 tumour-bearing mice receiving daily i.t. administration of PBS or MeβCD (1 mg per injection) only from day 9 to 13 serve as controls. At day 14, all mice were sacrificed, and spleens harvested from the mice were weighed and processed for flow cytometry analyses. Experimental scheme (**b**). Shown are spleen weight (**c**), counts of Pmel $CD8^+$ T-cells (**d**), frequency of polyfunctional $CD8^+$ T-cells (**e**) in spleens (n = 6 animals per group). Data are one representative of two independent experiments with biological replicates. *P* values were determined by one-way ANOVA. Error bars represent SEM. PBS, phosphate-buffered saline; n.s., not significant.

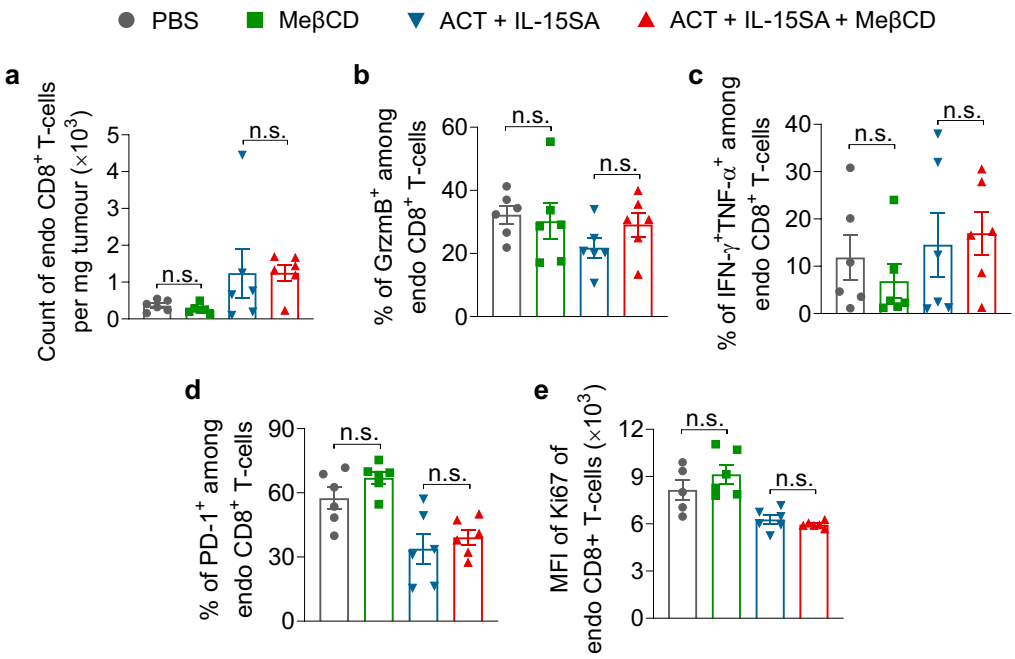


**Supplementary Figure 13**

**Treatment of MeβCD shows negligible effects on proliferation and functions of tumour-infiltrating endogenous (endo) CD8⁺ T-cells.**

**a-e**, B16F10 tumour-bearing mice received the same treatment as shown in supplementary Figure 12b. At day 14, mice were sacrificed, and tumours harvested from the mice were processed for flow cytometry analyses. Shown are counts of endo CD8⁺ T-cells (**a**), frequencies of granzyme B (GrzmB)⁺ (**b**), polyfunctional (**c**), and PD-1⁺ (**d**), and mean fluorescence intensity (MFI) of Ki67 (**e**) of endo CD8⁺ T-cells (n = 6 animals per group). Data are one representative of two independent experiments with biological replicates. *P* values were determined by one-way ANOVA. Error bars represent SEM. PBS, phosphate-buffered saline; n.s., not significant.

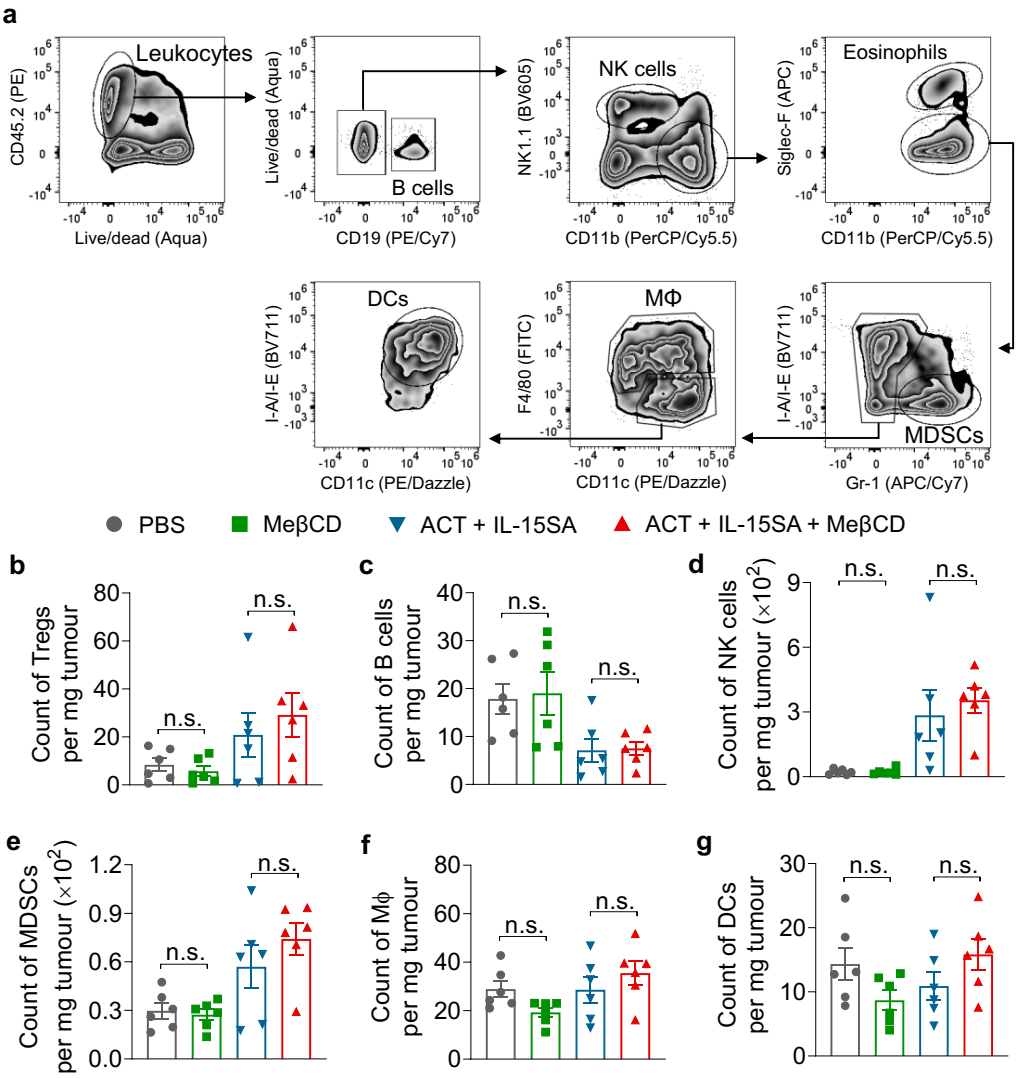


**Supplementary Figure 14**

**Treatment of MeβCD shows negligible effects on other tumour-infiltrating immune cells.**

**a-g**, B16F10 tumour-bearing mice received the same treatment as shown in supplementary Figure 12b. At day 14, mice were sacrificed, and tumours harvested from the mice were processed for flow cytometry analyses. **a**, Shown are the gating strategies for B cells, natural killer (NK) cells, eosinophils, myeloid-derived suppressor cells (MDSCs), macrophages (MΦ), and dendritic cells (DCs) in tumour. **b-g**, Shown are counts of regulatory T-cells (Tregs; $Foxp3^{+}CD4^{+}$ T-cells) (**b**), B cells (**c**), NK cells (**d**), MDSCs (**e**), MΦ (**f**), and DCs (**g**) infiltrating in tumours (n = 6 animals per group). Data are one representative of two independent experiments with biological replicates. *P* values were determined by one-way ANOVA. Error bars represent SEM. PBS, phosphate-buffered saline; n.s., not significant.

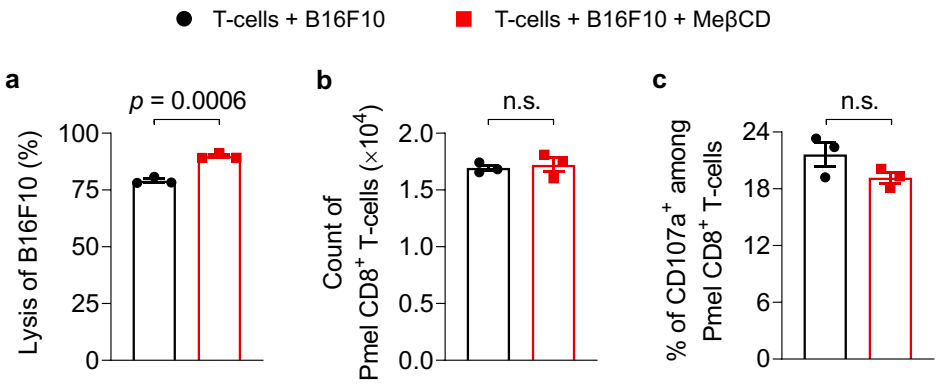


**Supplementary Figure 15**

**MeβCD shows negligible effects on T-cell functions during co-culture with cancer cells.**

**a**, Lysing percentage of B16F10 cancer cells after 48-h co-culture with Pmel CD8+ T-cells at an effector:target ratio of 1:1 in the presence of MeβCD (n = 3). **b**, **c**, Cell counts (**b**) and frequency of CD107+ (**c**) of Pmel CD8+ T-cells were analyzed by flow cytometry. Data are one representative of two independent experiments with biological replicates. *P* values were determined by unpaired Student's t test. Error bars represent SEM. n.s., not significant.

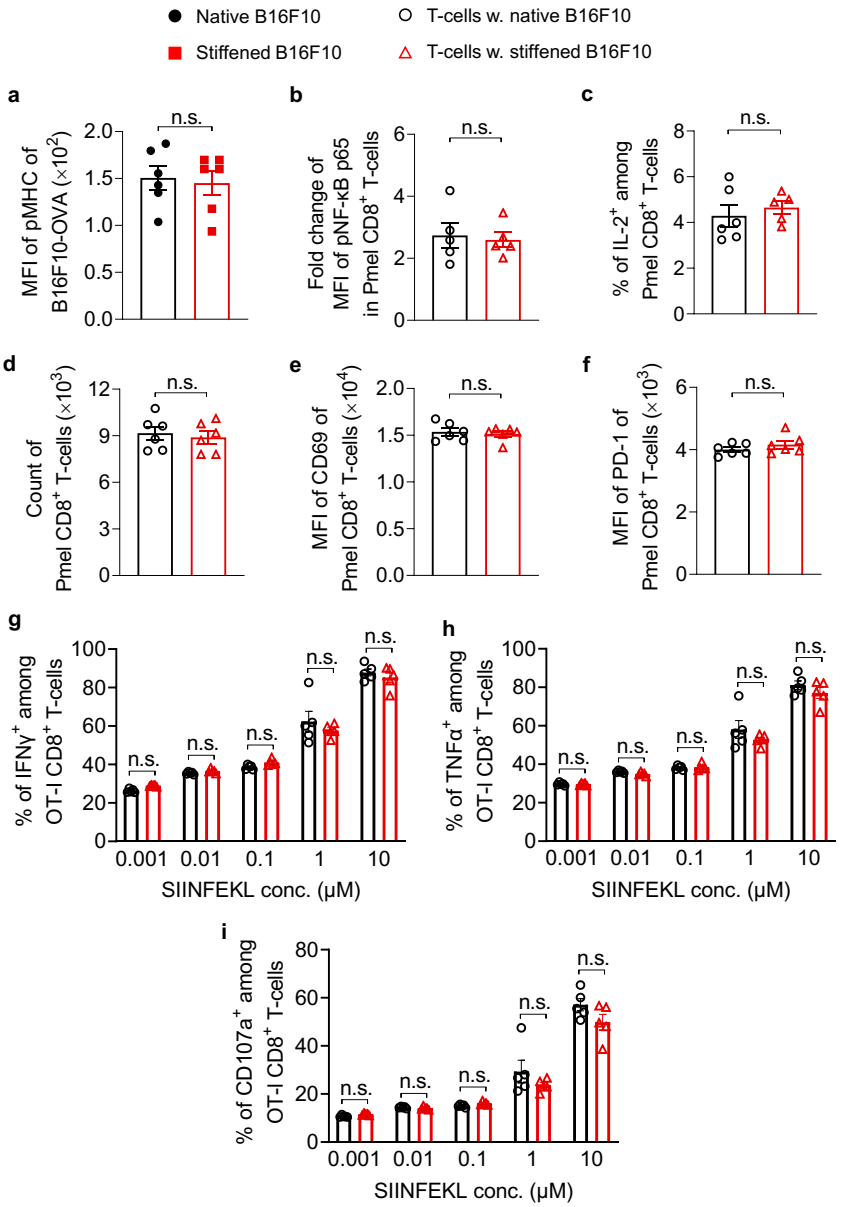


**Supplementary Figure 16**

**Cancer-cell stiffening using MeβCD shows negligible effects on antigen presentation by cancer cells, T-cell proliferation, activation or other phenotypes.**

**a**, SIINFEKL-MHC-I complex (pMHC) expression level on B16F10-OVA cancer cells after treatment with MeβCD (5 mM) at 37 °C for 30 min (n = 6). **b**, Fold change of mean fluorescence intensity (MFI) of phosphorylated NF-κB subunit p65 (pNF-κB p65) in activated Pmel CD8+ T-cells stimulated by MeβCD-treated (stiffened) B16F10 cancer cells at 37 °C for 5 min (n = 5). **c**-**f**, Activated Pmel CD8+ T-cells were co-cultured with stiffened B16F10 cancer cells at an effector:target (E:T) ratio of 10:1 for 5 h. Shown are IL-2+ percentage (**c**), count (**d**), and MFI of CD69 (**e**) and PD-1 (**f**) of Pmel CD8+ T-cells (n = 6). **g**-**i**, Activated OT-I CD8+ T-cells were co-cultured with stiffened B16F10 cancer cells (E:T ratio = 10:1) pulsed with various concentrations of SIINFEKL peptide at 37 °C for 5 h. Shown are frequencies of IFN-γ+ (**g**), TNF-α+ (**h**), and CD107a+ (**i**) of OT-I CD8+ T-cells (n = 6). Data are one representative of three independent experiments with biological replicates. *P* values were determined by unpaired Student's *t* test. Error bars represent SEM. conc., concentration; n.s., not significant.

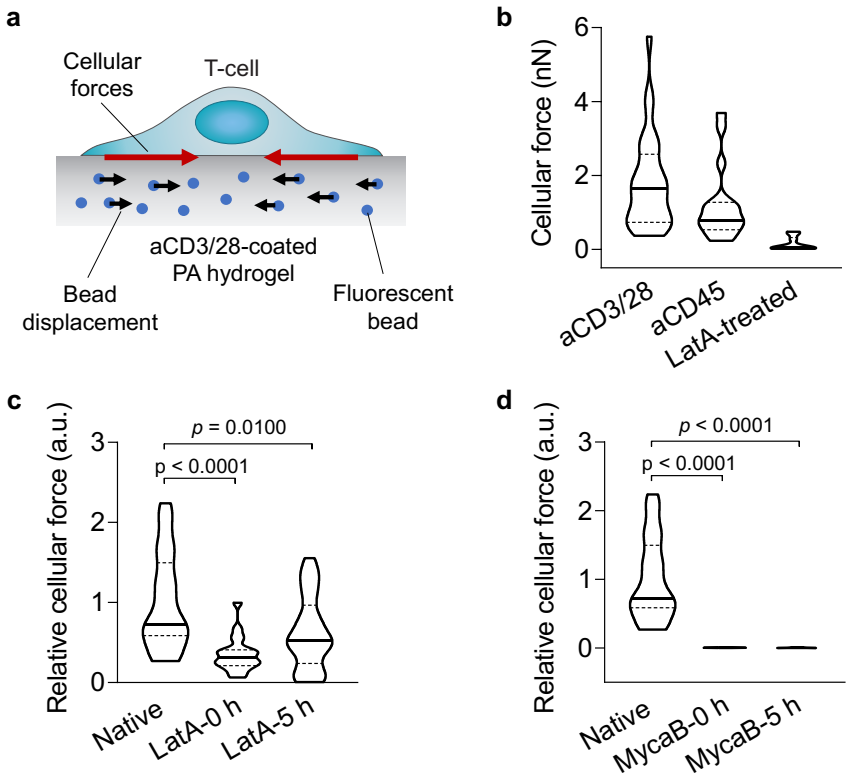


**Supplementary Figure 17**

**T-cell force is measured using traction force microscopy (TFM) and can be stably inhibited by applying cytoskeleton inhibitors.**

**a**, Schematic illustration of TFM measurement of T-cell forces on a PA hydrogel coated with anti-CD3/anti-CD28 antibodies (aCD3/28) and embedded with fluorescent beads. **b**, Average total forces per cell exerted by activated Pmel $CD8^+$ T-cells on a hydrogel substrate ($E$ = 890 Pa) coated with aCD3/28 (n = 29) or non-stimulatory anti-CD45 antibody (aCD45) (n = 17), or by T-cells pre-treated with Latrunculin A (LatA) on an aCD3/28-coated hydrogel substrate ($E$ = 890 Pa; n = 10). **c**, **d**, Relative total forces per cell exerted by T-cells on hydrogel substrate ($E$ = 890 Pa) coated with aCD3/28 (n = 27), or T-cells pre-treated with LatA (**c**) or mycalolide B (MycaB; **d**) at 0 h (n = 20 and 10 for LatA and MycaB, respectively) and 5 h (n = 29 and 8 for LatA and MycaB, respectively) post pre-treatment on the same substrate. In the violin plots, the middle solid line shows median, and lower and upper dash lines show $25^{th}$ and $75^{th}$ percentiles, respectively. Data are one representative of two independent experiments with biological replicates. $P$ values were determined by unpaired Student's t test. Error bars represent SEM. a.u., arbitrary unit.

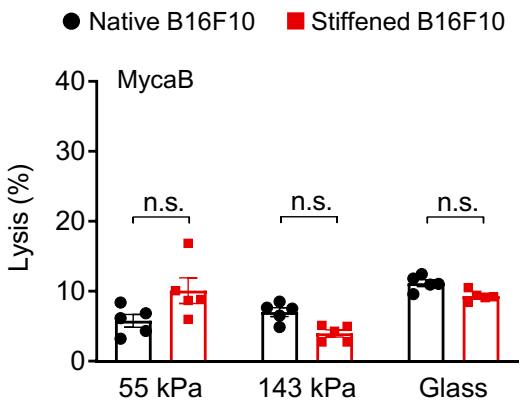


**Supplementary Figure 18**

**Enhanced T-cell cytotoxicity against stiffened target cells is mediated by T-cell forces.**

Lysis percentage of native and MeβCD-treated (stiffened) B16F10 cancer cells co-cultured with activated Pmel $CD8^+$ T-cells (effector:target ratio = 10:1), which were pre-treated with mycalolide B (MycaB) (n = 5). Data are one representative of two independent experiments with biological replicates. *P* values were determined by unpaired Student's *t* test. Error bars represent SEM. n.s., not significant.

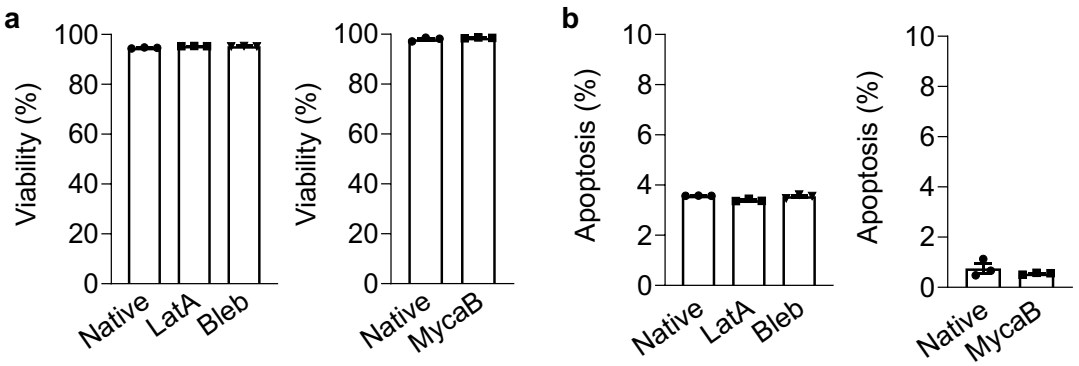


**Supplementary Figure 19**

**Treatment of cytoskeleton inhibitors shows negligible impacts on the viability or apoptosis of Pmel CD8+ T-cells.**

**a**, **b**, Percentages of viable (**a**) and apoptotic (**b**) Pmel CD8+ T-cells after the treatment with different cytoskeleton inhibitors (n = 3). LatA, latrunculin A; Bleb, blebbistatin; MycaB, mycalolide B. Data are one representative of two independent experiments with biological replicates. Error bars represent SEM.